








RESEARCH ARTICLE | JUNE 13 2023

Structural evolution and thermoelectric properties of $\text{Mg}_3\text{Sb}_x\text{Bi}_{2-x}$ thin films deposited by magnetron sputtering

Special Collection: [Celebrating the Achievements and Life of Joe Greene](#)

Grzegorz Sadowski ; Rui Shu ; Arnaud le Febvrier ; Zhijia Han ; Denis Music ; Weishu Liu ; Per Eklund 



J. Vac. Sci. Technol. A 41, 043409 (2023)

<https://doi.org/10.1116/6.0002635>



View
Online



Export
Citation

CrossMark



Instruments for Advanced Science

- Knowledge
- Experience
- Expertise

[Click to view our product catalogue](#)

Contact Hiden Analytical for further details:

www.HidenAnalytical.com

info@hiden.co.uk

Gas Analysis

- dynamic measurement of reaction gas streams
- catalysis and thermal analysis
- molecular beam studies
- dissolved species probes
- fermentation, environmental and ecological studies

Surface Science

- UHV/TPD
- SIMS
- end point detection in ion beam etch
- elemental imaging - surface mapping

Plasma Diagnostics

- plasma source characterization
- etch and deposition process reaction kinetic studies
- analysis of neutral and radical species

Vacuum Analysis

- partial pressure measurement and control of process gases
- reactive sputter process control
- vacuum diagnostics
- vacuum coating process monitoring

Structural evolution and thermoelectric properties of $\text{Mg}_3\text{Sb}_x\text{Bi}_{2-x}$ thin films deposited by magnetron sputtering

Cite as: J. Vac. Sci. Technol. A 41, 043409 (2023); doi: 10.1116/6.0002635

Submitted: 3 March 2023 · Accepted: 30 May 2023 ·

Published Online: 13 June 2023



Grzegorz Sadowski,^{1,2,a)} Rui Shu,² Arnaud le Febvrier,² Zhijia Han,³ Denis Music,^{1,4} Weishu Liu,^{3,5} and Per Eklund²

AFFILIATIONS

¹Department of Materials Science and Applied Mathematics, Malmö University, Malmö SE-205 06, Sweden

²Thin Film Physics Division, Department of Physics, Chemistry, and Biology (IFM), Linköping University, Linköping SE-581 83, Sweden

³Department of Materials Science and Engineering, Southern University of Science and Technology, Shenzhen, Guangdong 518055, China

⁴Biofilms Research Center for Biointerfaces, Malmö University, Malmö SE-205 06, Sweden

⁵Guangdong Provincial Key Laboratory of Functional Oxide Materials and Devices, Southern University of Science and Technology, Shenzhen, Guangdong 518055, China

Note: This paper is part of the Special Topic Collection Celebrating the Achievements and Life of Joe Greene.

^{a)}Electronic mail: grzegorz.sadowski@mau.se

ABSTRACT

$\text{Mg}_3\text{Bi}_{2-x}$ -based compounds are of great interest for thermoelectric applications near room temperature. Here, undoped p-type $\text{Mg}_3\text{Sb}_x\text{Bi}_{2-x}$ thin films were synthesized using magnetron sputtering (three elemental targets in Ar atmosphere) with a growth temperature of 200 °C on three different substrates, namely, Si as well as *c*- and *r*-sapphire. The elemental composition was measured with energy-dispersive x-ray spectroscopy and the structure by x-ray diffraction. The electrical resistivity and the Seebeck coefficient were determined under He atmosphere from room temperature to the growth temperature. All samples are crystalline exhibiting the La_2O_3 -type crystal structure (space group P-3m1). The observed thermoelectric response is consistent with a semiconductive behavior. With increasing *x*, the samples become more electrically resistive due to the increasing bandgap. High Bi content ($x < 1$) is thus beneficial due to lower resistivity and a higher power factor near room temperature. Thermoelectric thin films synthesized at low temperatures may provide novel pathways to enable flexible devices on polymeric and other heat-sensitive substrates.

© 2023 Author(s). All article content, except where otherwise noted, is licensed under a Creative Commons Attribution (CC BY) license (<http://creativecommons.org/licenses/by/4.0/>). <https://doi.org/10.1116/6.0002635>

I. INTRODUCTION

Thermoelectric thin films are suitable for energy generation and cooling microdevices, with the potential to have improved thermoelectric properties compared to bulk¹ with their low dimensionality yielding beneficial effects such as quantum confinement² and additional phonon scattering.³ The thermoelectric-based devices can be used for localized cooling of high heat-flux areas, self-powered sensors, as well as Internet of things devices.⁴

Room temperature (RT) thermoelectric materials are less explored than those operating at elevated temperatures. The bipolar effect is a known limiting factor for many thermoelectric materials. While larger bandgaps of high temperature thermoelectrics have a suppressing effect on it, the room temperature applications require small bandgaps close to 0.26 eV.⁵ Most middle-temperature thermoelectric materials exhibit a bandgap of at least 0.5 eV, which yields a good performance at high temperatures but hinders room temperature applications.⁵ Inorganic bismuth telluride compounds

10 January 2024 07:46:08

are well-established thermoelectric materials for applications near RT,¹ but their brittleness, as well as scarcity and high cost of Te limit their large-scale applications.⁶ An alternative to Bi₂Te₃ with better thermal stability is MgAsSb, but a complicated synthesis process and a relatively high electrical resistivity are limiting its current use.^{7,8} Cu₂Se is an unusual high temperature thermoelectric material that undergoes phase transition around 410 °C and possesses a high Seebeck coefficient below the transition,⁹ but its chemical stability is the main challenge. AgSbTe₂ is a system with a high Seebeck coefficient above 125 °C¹⁰ and low electrical resistivity, but again its stability requires improvements. Ag₂Se is another promising RT material without Te.¹¹ Clearly, there are many challenges for RT thermoelectric systems. As inorganic thermoelectric materials are often inherently rigid, there is a growing interest in combining the flexibility of organic materials with the thermoelectric properties of inorganic materials. One approach is to synthesize an inorganic thin film on a flexible substrate.⁷ Most polymeric substrates cannot withstand high temperatures¹²—low temperature synthesis is thus necessary.

The Zintl phase Mg₃Sb_xBi_{2-x} alloys with an La₂O₃-type crystal structure (space group P-3m1)^{13,14} are promising thermoelectric materials for applications at temperatures below 450 °C, which is the thermal stability limit of the material partly due to the high saturated vapor pressure of Mg.¹⁵ The constituent elements are relatively abundant and nontoxic. In 2016, it was shown¹⁵ that a slight excess in the Mg content and Te-doping can change Mg_{3+δ}Sb_{1.5}Bi_{0.49}Te_{0.01} from the p-type to n-type material with an improved thermoelectric figure of merit (ZT) of ~1.5 around 445 °C. For Mg₃Bi₂-based materials, n-type counterparts have better thermoelectric properties than p-type due to band structure modulations.¹⁶ It has been reported¹⁷ that n-type Mg₃Sb_{0.6}Bi_{1.4} possesses a ZT value superior to that of Bi₂Te₃ for temperatures between 125 and 225 °C, and that Mg_{3+δ}Sb_xBi_{2-x} can have comparable thermoelectric properties between 50 and 250 °C, making Mg₃Bi₂-based materials rather promising substitutes at RT.¹⁸ Recently, Bi-/Ge-rich Janus nanoprecipitates from local co-melting of Bi and Ge during sintering have been found to enable low lattice thermal conductivity near room temperature for Mg₃Sb_{1.5}Bi_{0.5}.¹⁹

For Mg₃Bi₂-based materials, the compositions close to Mg₃Sb_{1.5}Bi_{0.5} appear to be optimized to yield high ZT below 450 °C.¹⁵ Studies on p-type bulk materials have shown that alloying Mg₃Sb₂ and Mg₃Bi₂ reduces their thermal conductivity—the value for Mg₃Bi₂ at RT has been reported to be over three times higher and increasing in a linear fashion with temperature compared to almost temperature independent Mg₃SbBi.²⁰ The increased Bi content decreases the bandgap, shifting the optimal thermoelectric temperature to lower values but also increasing the bipolar effect.²¹ Semiconductors with narrow bandgaps are more prone to having a current composed of both holes and electrons (minority and majority carriers) at temperatures sufficient for thermal excitation, which diminishes the total Seebeck coefficient.²² Based on the literature for the n-type material, for applications around room temperature compositions between Mg₃SbBi and Mg₃Sb_{0.5}Bi_{1.5} may be of interest,¹⁶ while for temperatures close to 175 °C, the predicted optimal range changes to the composition between Mg₃SbBi and Mg₃Sb_{0.8}Bi_{1.2}, and Mg₃SbBi at 330 °C. With Cu and Te doping, as well as reduced grain boundary thermal resistance, Mg₃Sb_{0.5}Bi_{1.5}

achieved an average ZT above 1 in the temperature range between 50 and 150 °C.²³

The deposition process of thin films can offer a greater degree of control over the composition, structure, and strain of the material compared to bulk synthesis. Bulk Mg₃Sb_xBi_{2-x} has been a focus of many studies, and there is a growing interest in thermoelectric properties of Mg₃Bi₂ (Ref. 24) and Mg₃Sb₂ (Refs. 25–27) thin films. Investigating the structure evolution of undoped p-type Mg₃Sb_xBi_{2-x} is important for a better understanding of fundamental physical properties of this system and can be useful in improving the n-type material. Thermoelectric thin films synthesized at low temperatures also provide novel pathways to enable flexible devices on polymeric and other heat-sensitive substrates.²⁸

II. EXPERIMENT

Mg₃Sb_xBi_{2-x} thin films with x from 0 to 1.19 were deposited without doping using direct current (dc) magnetron sputtering in a vacuum chamber (base pressure < 4 × 10⁻⁶ Pa). A detailed description of the deposition system is available elsewhere.²⁹ Mg (99.99%, MaTeck), Sb (99.999%, Plasmaterials), and Bi (99.99%, Plasmaterials) circular elemental targets (50.8 mm in diameter) were driven by dc-power supplies. The Mg target power was fixed to 90 W, Sb target power was altered from 0 to 12 W, and Bi target power ranged from 15 to 6 W. The Ar gas flow rate was fixed to 80 SCCM corresponding to a working pressure of 0.5 Pa (3.75 mTorr). The heater was maintained at constant temperature and the substrate holder rotated at 15 rpm, with the substrates electrically floating. The heater temperature was calibrated to correspond to approximately 200 °C on the substrate. The deposition time was 15 min, yielding a thickness above 400 nm for all the thin films, as estimated based on target power, and the thickness of Mg₃Bi₂ and Mg₃Sb₂ films measured from cross sections using scanning electron microscopy (SEM). The films deposited on Si(100), *r*-sapphire, and *c*-sapphire 10 × 10 mm² substrates were used for structural characterization by x-ray diffraction (XRD) in a $\theta/2\theta$ setup with a spinner stage and a minimal step size 2θ : 0.001 and φ : 0.1° for in-plane rotation. The substrates were cleaned sequentially with acetone and ethanol in an ultrasonic bath for 10 min and, finally, blow-dried with nitrogen gas before deposition. The native oxides on Si substrates were not removed. An anode made of Cu and a Ni-filter was used. Elemental composition was determined by energy-dispersive x-ray spectroscopy (EDS) in a scanning electron microscope (SEM, Oxford Instruments X-Max, 20 keV). The electrical resistivity ρ , the Seebeck coefficient S , and the power factor S^2/ρ of films on *c*- and *r*-sapphire were measured by a commercial system (CTA-3) under a low-pressure helium atmosphere from RT to 200 °C (growth temperature).

III. RESULTS AND DISCUSSION

The EDS data were averaged from three separate areas for each sample, as measured on Si. The autofit function was used to label the peaks from the raw data, with oxygen peaks being excluded (possible contamination after exposure to air). As all the substrates were used for synthesis simultaneously, the composition on sapphire substrates is expected to be the same. To determine the thickness dependence on x, a growth rate of a sample with 38 at. %

10 January 2024 07:46:08

of Sb synthesized at room temperature was obtained. Hence, with the growth rate data, the thickness was estimated for all samples.

The growth temperature of 200 °C was chosen to obtain epitaxial growth for Mg_3Bi_2 , as investigated in our previous study, and to avoid loss of Mg observed already occurring with a substrate temperature of 300 °C.²⁴ The relatively low growth temperature can be useful for depositing on polymers and other flexible, temperature-sensitive samples. From the EDS data (Table I), it can be deduced that the Mg content is slightly over 60 at. % ($\delta > 0$). Te-doped $\text{Mg}_3\text{Sb}_x\text{Bi}_{2-x}$ ($x = 0.5, 1, 1.5$) samples were reported to have good thermal stability at 300 °C during a 50h annealing experiment,³⁰ sufficient for low-temperature applications. Hence, the compositional range of interest is systematically explored in the current work. For simplicity, δ is omitted henceforth. It should be noted that since the samples were exposed to atmosphere, a slight color change of the films due to oxidation of the surfaces of the samples was observed when the samples were visually inspected four weeks later. It has been reported that for long term stability, an additional surface layer and Mg-vapor annealing³¹ might be necessary.

Figure 1 contains the XRD patterns of $\text{Mg}_3\text{Sb}_x\text{Bi}_{2-x}$ films deposited on *c*- and *r*-sapphire as well as Si(100) for various Sb contents. On *c*-sapphire, the Mg_3Bi_2 sample ($x = 0$) is highly 0001 oriented. The orientation of the film with relation to the *c*-sapphire substrate is (0001) Mg_3Bi_2 || (0001) Al_2O_3 and [11 $\bar{2}$ 0] Mg_3Bi_2 || [11 $\bar{2}$ 0] Al_2O_3 , as determined previously using pole figures and confirmed by the density functional theory.²⁴ Addition of Sb ($x > 0$) clearly modifies the crystalline structure. The reported lattice constant *a* of Mg_3Bi_2 is 4.675 Å and *c* is 7.416 Å,³² while the lattice constants of Mg_3Sb_2 are 4.584 and 7.274 Å, respectively.³³ Since the linear coefficients of thermal expansion for Al_2O_3 (15.7 ppm/K)³⁴ and $\text{Mg}_3(\text{Sb},\text{Bi})_2$ (22.3 ppm/K)³⁵ are quite similar, it is not expected to have significant thermal stresses for the samples grown at 200 °C. Hence, the lattice parameters should not be affected by the thermal stress state to a high extent. Based on the fitting of high-intensity XRD peaks (11 $\bar{2}$ 0 and 0003), the *a* and *c* lattice parameters decrease from 4.673 and 7.399 Å at $x = 0$ to 4.634 and 7.356 Å at $x = 0.43$ and to 4.584 and 7.069 Å at $x = 0.81$, respectively. This trend supports the notion of Sb incorporation in the lattice and is consistent with the literature.³² Furthermore, point defects may also affect the estimated lattice parameters.

TABLE I. Composition of the $\text{Mg}_{3+\delta}\text{Sb}_x\text{Bi}_{2-x}$ samples obtained from EDS experiments, where δ represents extra Mg, the total content of Sb and Bi is set to 2, and *x* is the ratio of alloying Sb over the sum of Sb and Bi. The error is represented by standard deviation between the results from the three investigated areas on each sample. The thickness was estimated based on Mg_3Bi_2 and Mg_3Sb_2 samples, as measured by cross section of the films measured in SEM.

Sample	δ	<i>x</i>	2 − <i>x</i>	Estimated thickness (nm)
1	0.04 ± 0.01	0.00 ± 0.00	2.00 ± 0.00	407
2	0.05 ± 0.01	0.43 ± 0.01	1.57 ± 0.01	425
3	0.03 ± 0.01	0.81 ± 0.01	1.19 ± 0.01	444
4	0.04 ± 0.01	1.00 ± 0.01	1.00 ± 0.01	453
5	0.04 ± 0.01	1.19 ± 0.01	0.81 ± 0.01	463

The increase of the Sb content results in a slight decrease of the lattice parameter, which can be observed as peaks move toward higher angles. With the rise of Sb content, the intensity of 0001 peaks decreases while other peaks (1010, 2020, 1122, and 1233) increase.

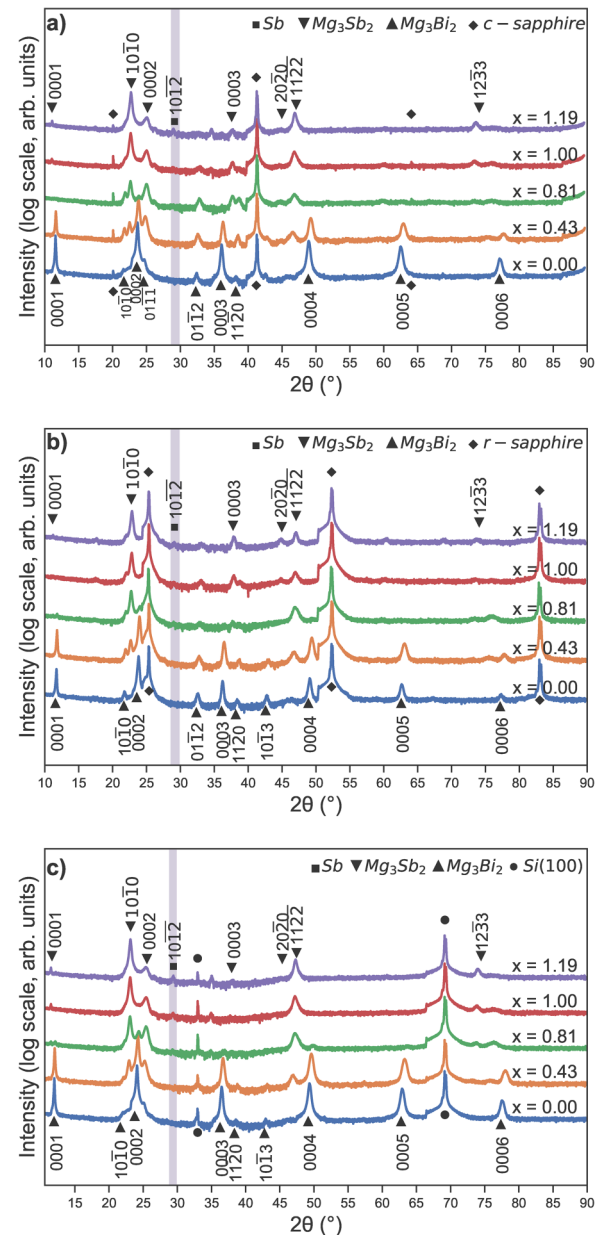
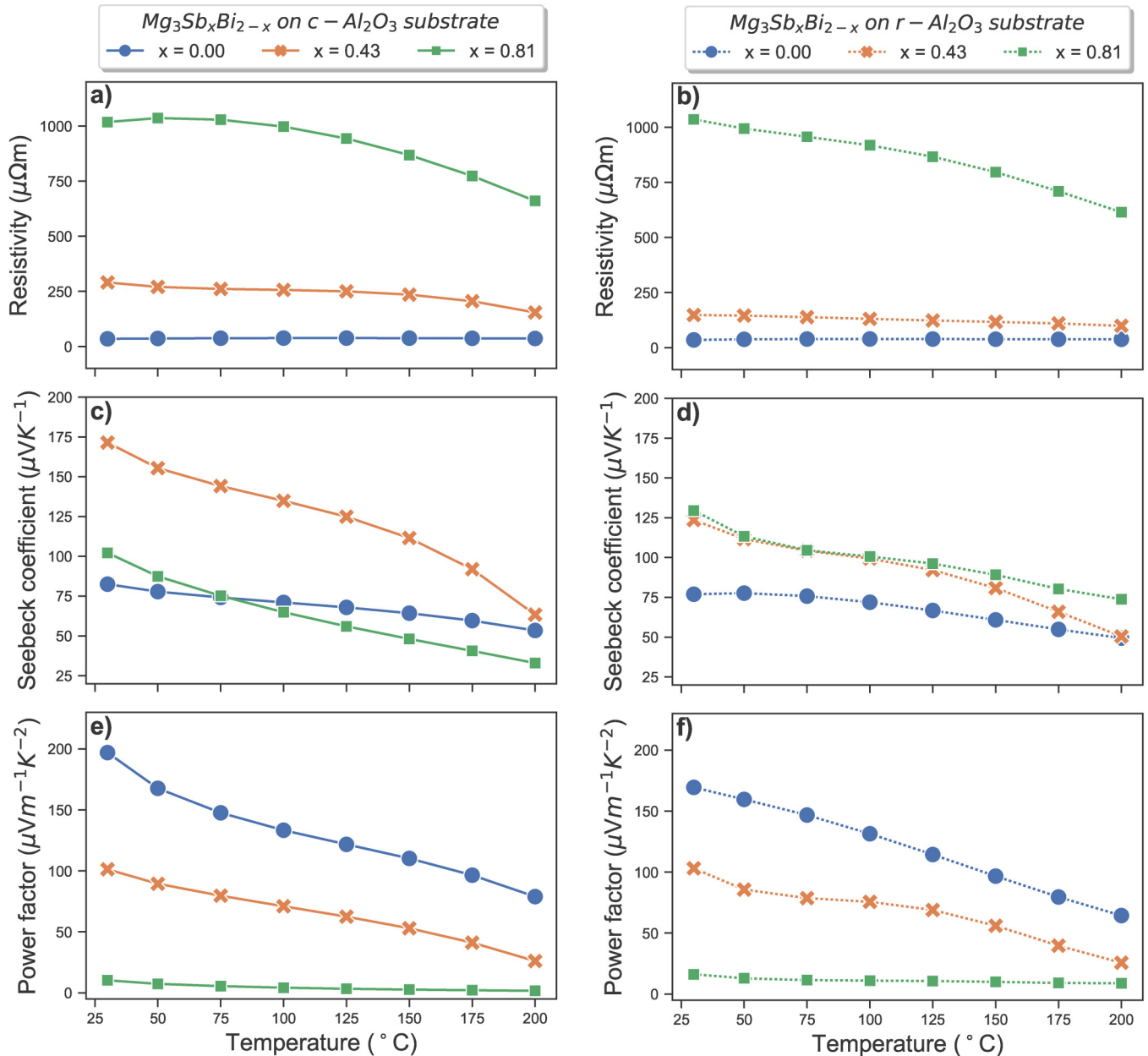


FIG. 1. X-ray diffraction patterns of $\text{Mg}_3\text{Sb}_x\text{Bi}_{2-x}$ with different Sb/Bi ratios grown at 200 °C on (a) *c*-sapphire, (b) *r*-sapphire, and (c) Si(100) substrate. The highlighted region indicates the range in which the precipitation of Sb can occur. Thermoelectric properties of the Mg_3Bi_2 sample were investigated (Ref. 24) in a previous study.



10 January 2024 07:46:08

FIG. 2. (a) and (b) Resistivity, (c) and (d) the Seebeck coefficient, (e) and (f) power factor of $\text{Mg}_3\text{Sb}_x\text{Bi}_{2-x}$ grown on *c*-sapphire and *r*-sapphire as a function of temperature.

associated with the solid solution of $\text{Mg}_3\text{Sb}_{2-x}\text{Bi}_x$ appear as the films become increasingly polycrystalline. A similar pattern has been also observed for films grown on Si(100) and *r*-sapphire substrates (Fig. 1). Observing the crystal structure of $\text{Mg}_3\text{Sb}_x\text{Bi}_{2-x}$ grown on Si substrates provides information on how a substrate induces structural and microstructural modulations, which may be of significance for future experiments. The 1012 Sb peak appears

for Sb-rich compositions (the highlighted peak in Fig. 1). The appearance of a similar Sb peak has been reported for Mg_3Sb_2 synthesized without excess of Mg to offset Mg loss due to a high synthesis temperature (800 °C).³⁶ This might imply that there is a minute deficiency of Mg in our Sb-rich samples, despite EDS measurements showing the content to be slightly over 60 at. %. Considering all the data in Fig. 1 regarding the phase purity (no

metallic Sb precipitations), only the samples with $x < 1$ are further analyzed in terms of the transport properties.

Figure 2 presents temperature-dependent electrical resistivity, the Seebeck coefficient, and the power factor of $\text{Mg}_3\text{Sb}_x\text{Bi}_{2-x}$ films for $x < 1$. Due to the variations in the estimated thickness of the films, the actual resistivity for $x > 0$ may be up to 10% lower than the presented data. The thermoelectric properties of films grown on Si substrates are not measured, since the Si substrate dominates any such measurements, which are not representative of the films. For thermoelectric property measurements, films synthesized on an insulating substrate are required. It can be observed that the lower Sb content yields lower electrical resistivity [Figs. 2(a) and 2(b)]. This can be understood by considering the semimetallic nature of Mg_3Bi_2 and the semiconductor nature of Mg_3Sb_2 .²⁰ $\text{Mg}_3\text{Sb}_x\text{Bi}_{2-x}$ ($x > 0$) is a semiconductor with higher Sb content expected to increase the electrical resistivity by enlarging the bandgap,²⁰ as observed herein. The Bi-rich samples may be limited by the high bipolar effect,¹⁶ which would increase with temperature. This explanation corresponds to the decrease in S at higher temperatures as observed in Figs. 2(c) and 2(d). As can be seen in Figs. 2(e) and 2(f), the two most Bi-rich samples (low value of x) in this study have the highest power factor, decreasing with temperature, with Mg_3Bi_2 having almost twice as large power factor as $\text{Mg}_3\text{Sb}_{0.43}\text{Bi}_{1.57}$ at RT. $\text{Mg}_3\text{Sb}_{0.81}\text{Bi}_{1.19}$ has relatively high electrical resistivity combined with the low Seebeck coefficient, similar to the Mg_3Bi_2 sample, despite its much lower Bi content, resulting in the lowest power factor of all samples. Similar trends are observed for the films grown on both *c*-sapphire (Fig. 2, left panel) and *r*-sapphire (Fig. 2, right panel), adding more certainty to the observations. Slight difference in the microstructures of the films grown on different substrates may result in a minute variation in the electrical properties. The differences are interesting but exploring them in more detail is beyond the scope of the current work.

Comparing the resistivity values for Mg_3Bi_2 thin film and bulk at RT, the values for thin films in the present study are considerably higher than the literature values for bulk materials²⁰—at room temperature, p-type bulk Mg_3Bi_2 was reported to have electrical resistivity of $5\ \mu\Omega\text{m}$, and the value of $\sim 10\ \mu\Omega\text{m}$ was claimed for $\text{Mg}_3\text{Sb}_{0.3}\text{Bi}_{1.7}$. For comparison, an undoped n-type bulk Bi_2Te_3 exhibits electrical resistivity of $6\ \mu\Omega\text{m}$ and the Seebeck coefficient of $-105\ \mu\text{V/K}$ at room temperature.^{7,37} A synthesis method can significantly affect the microstructure and change the populations and type of defects and impurities, which may be used to explain the difference, but this is beyond the scope of the current study.

IV. SUMMARY AND CONCLUSIONS

In conclusion, we investigated thermoelectric properties of the undoped p-type $\text{Mg}_3\text{Sb}_x\text{Bi}_{2-x}$ thin films deposited by magnetron sputtering on *c*-sapphire and *r*-sapphire substrates in a temperature range between RT and 200 °C. At $x \geq 1$, Sb precipitates, limiting the exploration of the transport properties to the thin film samples with $x < 1$. While the Mg_3Bi_2 sample is semimetallic, adding Sb content shifts the nature of the sample to a semiconductor, increasing the electrical resistivity and the Seebeck coefficient. High Bi content is favorable for applications near room temperature. This

work has prospects for synthesis and further study of $\text{Mg}_3\text{Bi}_{2-x}\text{Sb}_x$ thermoelectric thin films for applications below 200 °C.

ACKNOWLEDGMENTS

The work was supported financially by the Swedish Government Strategic Research Area in Materials Science on Functional Materials at Linköping University (Faculty Grant SFO-Mat-LiU No. 2009 00971), the Knut and Alice Wallenberg Foundation through the Wallenberg Academy Fellows Program (No. KAW-2020.0196), the Swedish Research Council (VR) under Project Nos. 2016-03365 and 2021-03826, the Olle Engkvist Foundation under Project No. 217-0023, the National Key Research and Development Program of China under Grant No. 2018YFB0703600, the National Natural Science Foundation of China (NNSFC) under Grant No. 51872133, Guangdong Innovative and Entrepreneurial Research Team Program under Grant No. 2016ZT06G587, the Tencent Foundation through the XPLOER PRIZE, and Guangdong Provincial Key Laboratory Program (No. 2021B1212040001) from the Department of Science and Technology of Guangdong Province. The authors acknowledge Yongbin Zhu for providing help with characterization and useful discussion.

AUTHOR DECLARATIONS

Conflict of Interest

The authors declare no competing interests.

Author Contributions

Grzegorz Sadowski: Investigation (equal); Visualization (lead); Writing – original draft (equal); Writing – review & editing (equal). **Rui Shu:** Conceptualization (equal); Investigation (equal); Writing – original draft (equal); Writing – review & editing (equal). **Arnaud le Febvrier:** Investigation (supporting); Supervision (equal); Writing – review & editing (equal). **Zhijia Han:** Investigation (equal); Writing – review & editing (equal). **Denis Music:** Formal analysis (supporting); Writing – review & editing (equal). **Weishu Liu:** Resources (equal); Supervision (equal); Writing – review & editing (equal). **Per Eklund:** Conceptualization (lead); Funding acquisition (lead); Investigation (supporting); Supervision (lead); Writing – original draft (equal); Writing – review & editing (equal).

DATA AVAILABILITY

The data that support the findings of this study are available within the article or are available from the corresponding author upon reasonable request.

REFERENCES

1. Venkatasubramanian, E. Siivola, T. Colpitts, and B. O'Quinn, *Nature* **413**, 597 (2001).
2. L. D. Hicks and M. S. Dresselhaus, *Phys. Rev. B* **47**, 12727 (1993).
3. W. Liu, J. Hu, S. Zhang, M. Deng, C.-G. Han, and Y. Liu, *Mater. Today Phys.* **1**, 50 (2017).

- ⁴I. Chowdhury, R. Prasher, K. Lofgreen, G. Chrysler, S. Narasimhan, R. Mahajan, D. Koester, R. Alley, and R. Venkatasubramanian, *Nat. Nanotechnol.* **4**, 235 (2009).
- ⁵Z. Han, J.-W. Li, F. Jiang, J. Xia, B.-P. Zhang, J.-F. Li, and W. Liu, *J. Materiomics* **8**, 427 (2022).
- ⁶J. Mao, G. Chen, and Z. Ren, *Nat. Mater.* **20**, 454 (2021).
- ⁷Z. Soleimani, S. Zoras, B. Ceranic, S. Shahzad, and Y. Cui, *Sustain. Energy Technol. Assess.* **37**, 100604 (2020).
- ⁸Y. Zheng *et al.*, *RSC Adv.* **8**, 35353 (2018).
- ⁹W.-D. Liu, L. Yang, and Z.-G. Chen, *Nano Today* **35**, 100938 (2020).
- ¹⁰K. Yu *et al.*, *Geomech. Geophys. Geo-Energy Geo-Resour.* **6**, 12 (2020).
- ¹¹J. A. Perez-Taborda, O. Caballero-Calero, L. Vera-Londono, F. Briones, and M. Martin-Gonzalez, *Adv. Energy Mater.* **8**, 1702024 (2018).
- ¹²Y. Du, J. Xu, B. Paul, and P. Eklund, *Appl. Mater. Today* **12**, 366 (2018).
- ¹³Y. Imai and A. Watanabe, *J. Mater. Sci.* **41**, 2435 (2006).
- ¹⁴T.-R. Chang *et al.*, *Adva. Sci.* **6**, 1800897 (2019).
- ¹⁵H. Tamaki, H. K. Sato, and T. Kanno, *Adv. Mater.* **28**, 10182 (2016).
- ¹⁶X. Shi *et al.*, *Mater. Today Phys.* **18**, 100362 (2021).
- ¹⁷K. Imasato, S. D. Kang, and G. J. Snyder, *Energy Environ. Sci.* **12**, 965 (2019).
- ¹⁸R. Shu *et al.*, *Adv. Funct. Mater.* **29**, 1807235 (2019).
- ¹⁹R. Shu *et al.*, *Adv. Sci.* **9**, 2202594 (2022).
- ²⁰V. Ponnambalam and D. T. Morelli, *J. Electron. Mater.* **42**, 1307 (2013).
- ²¹K. Imasato, S. D. Kang, S. Ohno, and G. J. Snyder, *Mater. Horiz.* **5**, 59 (2018).
- ²²L. Zhang, P. Xiao, L. Shi, G. Henkelman, J. B. Goodenough, and J. Zhou, *J. Appl. Phys.* **117**, 155103 (2015).
- ²³Z. Liu, W. Gao, H. Oshima, K. Nagase, C.-H. Lee, and T. Mori, *Nat. Commun.* **13**, 1120 (2022).
- ²⁴G. Sadowski, Y. Zhu, R. Shu, T. Feng, A. le Febvrier, D. Music, W. Liu, and P. Eklund, *Appl. Phys. Lett.* **120**, 051901 (2022).
- ²⁵S. Huang, Z. Wang, R. Xiong, H. Yu, and J. Shi, *Nano Energy* **62**, 212 (2019).
- ²⁶Z. Chang *et al.*, *Front. Mech. Eng.* **8**, 876655 (2022).
- ²⁷J.-I. Tani and H. Ishikawa, *J. Mater. Sci.: Mater. Electron.* **32**, 19499 (2021).
- ²⁸Y. Wang, L. Yang, X.-L. Shi, X. Shi, L. Chen, M. S. Dargusch, J. Zou, and Z.-G. Chen, *Adv. Mater.* **31**, 1807916 (2019).
- ²⁹A. le Febvrier, L. Landälv, T. Liersch, D. Sandmark, P. Sandström, and P. Eklund, *Vacuum* **187**, 110137 (2021).
- ³⁰H. Shang, Z. Liang, C. Xu, S. Song, D. Huang, H. Gu, J. Mao, Z. Ren, and F. Ding, *Acta Mater.* **201**, 572 (2020).
- ³¹J. Zhang, L. R. Jørgensen, L. Song, and B. B. Iversen, *ACS Appl. Mater. Interfaces* **14**, 31024 (2022).
- ³²T. Zhou, M. Tong, Y. Zhang, X. Xie, Z.-Y. Wang, T. Jiang, X.-G. Zhu, and X.-C. Lai, *Phys. Rev. B* **103**, 125405 (2021).
- ³³S. Song, J. Mao, J. Shuai, H. Zhu, Z. Ren, U. Saparamadu, Z. Tang, B. Wang, and Z. Ren, *Appl. Phys. Lett.* **112**, 092103 (2018).
- ³⁴M. Catti and A. Pavese, *Acta Crystallogr., Sect. B: Struct. Sci.* **54**, 741 (1998).
- ³⁵M. T. Agne *et al.*, *Mater. Today Phys.* **6**, 83 (2018).
- ³⁶C. L. Condon, S. M. Kauzlarich, F. Gascoin, and G. J. Snyder, *J. Solid State Chem.* **179**, 2252 (2006).
- ³⁷X. Wang *et al.*, *J. Mater. Sci.* **54**, 4788 (2019).